33RD INTERNATIONAL COSMIC RAY CONFERENCE, RIO DE JANEIRO 2013
THE ASTROPARTICLE PHYSICS CONFERENCE

ICRC 2013

CALET Positron/Electron Measurements Using the Geomagnetic Field

B. F. RAUCH[1] FOR THE CALET COLLABORATION.

[1] *Department of Physics and McDonnell Center for the Space Sciences, Washington University in St. Louis*

brauch@physics.wustl.edu

Abstract: The CALorimetric Electron Telescope (CALET) is under construction for launch to the International Space Station (ISS) in 2014, and consists of the main calorimeter (CAL) instrument and a dedicated Gamma-ray Burst Monitor (CGBM). The primary science goals of the CAL are to measure electron energy spectra from 1 GeV to 20 TeV, to detect gamma-rays above 10 GeV, and to measure the energy spectra of nuclei from protons through iron up to 1,000 TeV. In this paper we describe how Earth's geomagnetic field at the 51.6° inclination orbit of the ISS can be used to allow CAL to measure the distinct electron and positron fluxes. The positron to electron ratio has been seen to rise above $\sim$ 10 GeV by previous experiments (HEAT, AMS), and more recently to continue to increase to higher energies ($\sim$ 80 GeV for PAMELA, $\sim$ 200 GeV for Fermi, and $\sim$ 350 GeV with the best statistics for AMS-02). Utilizing the Earth shadow of the geomagnetic field the CAL will be able to distinguish electrons and positrons above an energy threshold of $\sim$ 3 GeV up to $\sim$ 20 GeV with favorable statistics compared to previous measurements before AMS-02, which includes the energy range where the positron to electron ratio turns over.

Keywords: CALET, cosmic ray, positrons, electrons, positron ratio.

1 Introduction

The positron fraction was first seen to rise at $\sim$ 10 GeV by HEAT [1] and AMS [2], and most recently it has been seen to continue to increase to higher energies $\sim$ 80 GeV for PAMELA [3, 4], $\sim$ 200 GeV for Fermi [5], and $\sim$ 350 GeV with the best statistics for AMS-02 [6], as shown in Fig. 1. The observation of a rising positron fraction has generally been attributed to possible spectral contributions from pulsars, or to dark matter annihilation, but [7] show that this feature could arise from cosmic ray propagation effects. The recent AMS results are consistent with those from PAMELA, but show those of Fermi to be systematically offset to higher values. AMS and PAMELA are both magnetic spectrometer instruments, while Fermi measured the positron fraction by exploiting the East-West effect of the geomagnetic field. The CALorimetric Electron Telescope (CALET) can employ the same technique used by Fermi to measure the positron to electron ratio, but in a lower energy range due to the fact that CALET on the ISS always points to zenith while Fermi can point near the horizon [8].

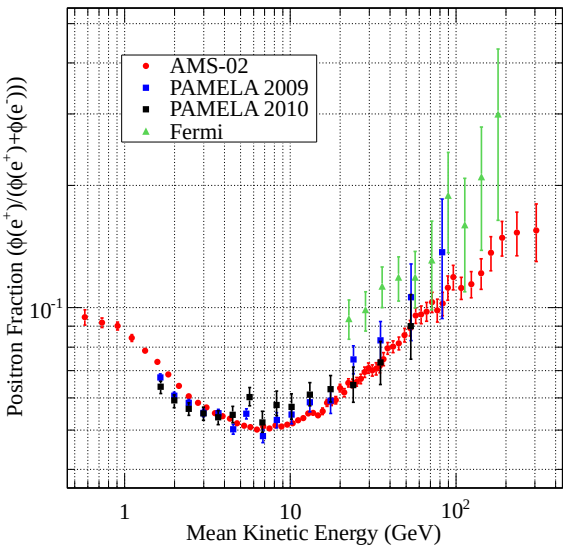

Figure 1: AMS [6], PAMELA [3, 4] and Fermi [5] positron fraction energy spectra.

2 CALET Instrument and Objectives

CALET is an experiment designed principally for the detection of the highest energy electrons. An instrument overview is given in [9], and its main scientific objectives are presented in [10, 11, 12]. CALET is under construction for launch to the International Space Station (ISS) in 2014, and it consists of the main calorimeter (CAL) and dedicated Gamma-ray Burst Monitor (CGBM) subsystems [13]. The CAL is shown in Fig. 2, and it consists from top to bottom of a charge detection module (CHD) composed of two crossed layers of 3.2 cm wide $\times$ 1 cm thick $\times$ 45 cm long EJ200 scintillator paddles, an imaging calorimeter (IMC) composed of eight x-y planes of 448 1 mm^2 scintillating fibers interleaved with tungsten plates, and a total absorption calorimeter (TASC) with twelve crossed layers of 16 19 mm wide $\times$ 20 mm tall $\times$ 326 mm long PWO logs. The IMC has 5 plates of 0.2 radiation length $X_\circ$ thick above 2 plates of 1 $X_\circ$ thick tungsten (total of 3 $X_\circ$) spaced with structural honeycomb, and the TASC has 27 $X_\circ$ of PWO, giving the CAL a total of 30 $X_\circ$ and making it the deepest calorimeter yet flown in space. The active area of the CAL decreases from 45 cm on a side at the CHD and IMC to 32 cm on a side in the TASC, and has a total instrument geometry factor of 0.12 m^{2}sr.

Due to the great depth of the TASC, the CAL will measure electrons with energies from 1 GeV up to 20 TeV.

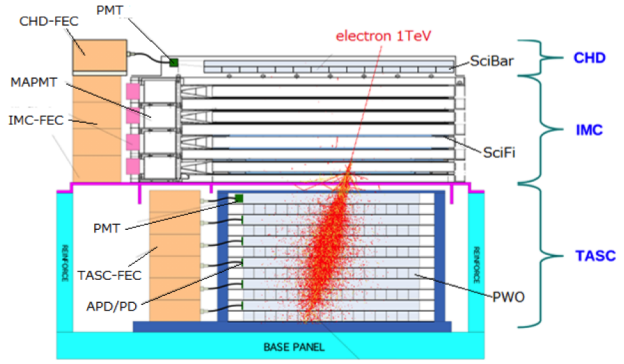

Figure 2: CAL side-view showing CHD, IMC, and TASC detectors.

CAL will also measure gamma-rays with energies between 10 GeV and 10 TeV, and the CHD has the charge resolution [14, 15] for the CAL to measure the energy spectra of the more abundant nuclei with $Z \leq 28$. In addition to the spectra of the more abundant Galactic cosmic ray (GCR) nuclei, CAL can measure the relative abundances of the rare ultra-heavy (UH) GCR utilizing the earth's magnetic field to select events above an energy threshold near minimum ionization in the CHD scintillators [16, 17, 18]. Similarly, CAL will be able to distinguish between electrons and positrons utilizing the earth shadow of the geomagnetic field, and will be able to measure their fluxes in the $\sim 3-20$ GeV energy range where the positron to electron ratio turns over, with favorable statistics to PAMELA and Fermi measurements in this range but not compared with AMS-02.

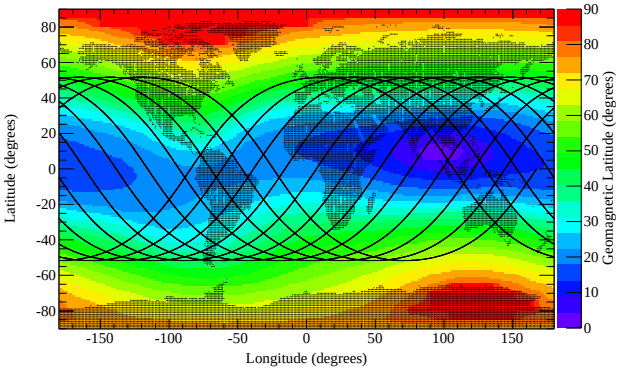

Figure 3: Geomagnetic latitudes derived from [19] vertical cutoff rigidities. Black curves show ISS orbit.

3 Analysis

3.1 Geomagnetic Exposure

Estimating the positron and electron fluxes that CALET will measure first requires determining the fraction of time it will spend as a function of geomagnetic latitude in its 51.6° inclination orbit on the ISS. Fig. 3 shows the geomagnetic latitude as a function of geographic coordinates, where the black curves show the ISS orbit path. It was derived from the vertical cutoff rigidities in [19] by interpolating to a 1° pitch and converting to geomagnetic latitude using Störmer theory: $R_{cut} = 15\cos^4(\lambda)$ GV, where λ is the geomagnetic latitude. The orbital residence time as a function of geographic latitude shown on the left in Fig. 4 is used to weight the geomagnetic latitudes that CALET will see in its orbit, which yields the orbit fraction CALET will spend as a function of geomagnetic latitude that is shown on the right in Fig. 4. The differential geometry factor of CALET as a function of East-West angle (γ, relative to West vector) for the triggering geometry of the CAL (IMC layers 7 and 8) and full TASC shown in Fig. 5 is used to determine the East-West angle exposure of the CAL, which is seen to peak at $\gamma = 90°$ because in the fixed orientation of the CAL on the ISS its normal points to the zenith.

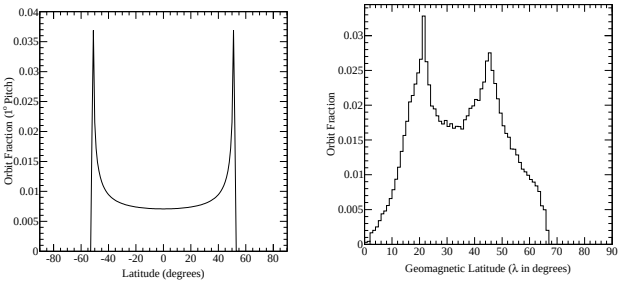

Figure 4: Left: ISS orbit fraction distribution for geographic latitudes. Right: Geomagnetic latitude residence time for CALET.

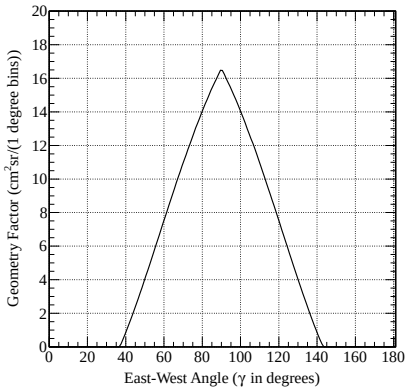

Figure 5: Differential geometry factor as a function of East-West angle (West $\gamma = 0$) for CALET triggering geometry (IMC layers 7 and 8) and full TASC.

3.2 Momentum Cutoffs

Störmer theory is used to predict the East-West angle and energy ranges where electrons and positrons can be separately resolved. The formulas for the critical momenta that define the minimum particle momentum (GeV/c) required to penetrate the earth's magnetic field as a function of geomagnetic latitude (λ) and East-West angle (γ) are given in Eqs. 1 and 2 for electrons and positrons, respectively. Figs. 6 and 7 show the critical momentum distributions for electrons and positrons, respectively. The opposite dependence of $p_{crit\ e^-}$ and $p_{crit\ e^+}$ on γ means that there are East-West angle and energy bands where only electrons or positrons can penetrate the earth's magnetic field.

$$p_{crit\ e^-}(\gamma,\lambda) = 60\left[\frac{1-\sqrt{1-\cos(\pi-\gamma)\cos^3(\lambda)}}{\cos(\pi-\gamma)\cos(\lambda)}\right]^2 \quad (1)$$

$$p_{crit\ e^+}(\gamma,\lambda) = 60\left[\frac{1-\sqrt{1-\cos(\gamma)\cos^3(\lambda)}}{\cos(\gamma)\cos(\lambda)}\right]^2 \quad (2)$$

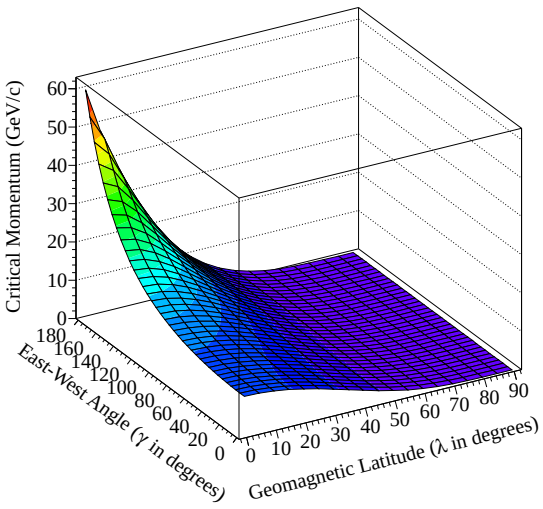

Figure 6: Electron critical momentum as a function of East-West angle (γ) and geomagnetic latitude (λ).

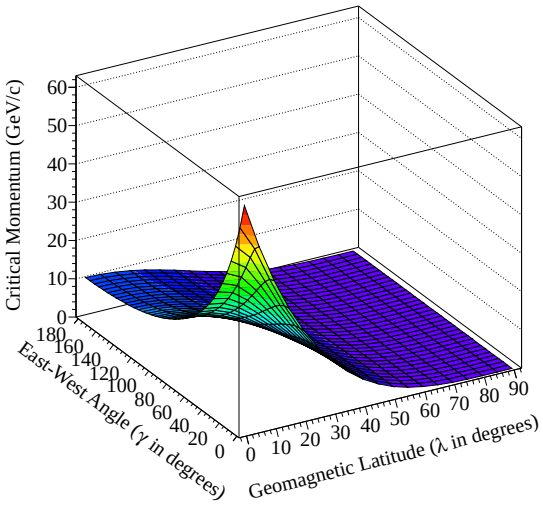

Figure 7: Positron critical momentum as a function of East-West angle (γ) and geomagnetic latitude (λ).

3.3 Electron and Positron Spectra

Fig. 8 shows the PAMELA electron flux [20] and the positron flux (AMS [6] with PAMELA [20]) used in this analysis multiplied by the cube of the particle energy (E^3), and clearly show the relative rise of the positron flux. The PAMELA positron flux derived from its published electron flux [20] and positron fraction [3] is compared with that taken from graph in [21], and is seen to agree within the combined error bars of the derived flux. The same approach was used to derive the positron flux using the AMS-02 positron fraction and the PAMELA electron flux that is used in this analysis.

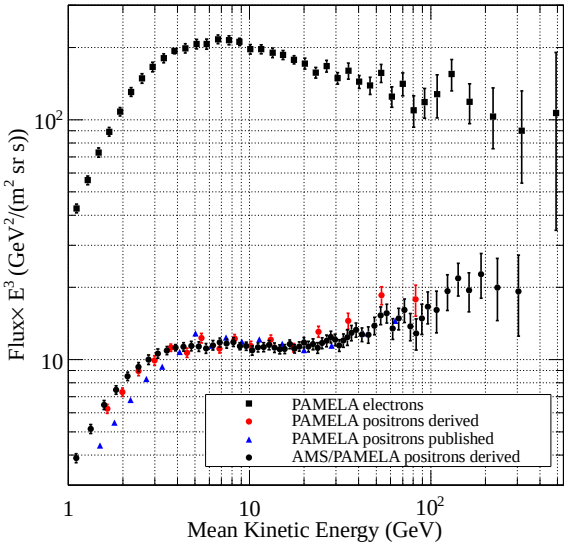

Figure 8: PAMELA electron and positron fluxes multiplied by the cube of the particle energy, E^3 [20, 3, 21].

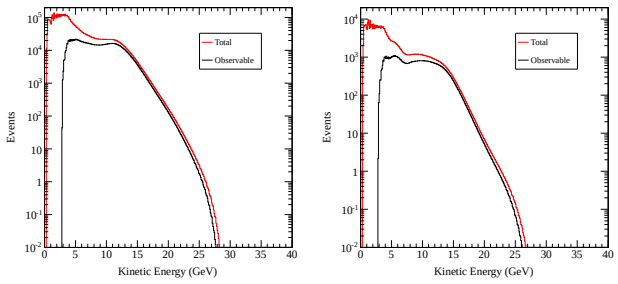

Figure 9: Comparison of incident and discernible fluxes in the CAL for electrons (left) and positrons (right).

3.4 Discernible Electron and Positron Fluxes

The differential geometry factor and East-West cutoff windows are used to predict the numbers of electron and positron events that will pass through CAL's acceptance over a 5 year mission as a function of energy, which are shown as the black curves in Fig. 9. The numbers of distinct electrons and positrons that CALET can resolve is limited by the instrument's detection efficiency and energy resolution, which are shown on the left and right, respectively, in Fig. 10 [22]. The event statistics that we expect CALET to see are estimated by multiplying the incident fluxes by the electron detection efficiency and narrowing the energy acceptance window at the high and low ends by the associated energy resolutions, with the result shown by the red curves in Fig. 9. The CAL detection efficiency and energy resolution limit the observable statistics at lower energies, and the geometric constraint on incidence angles

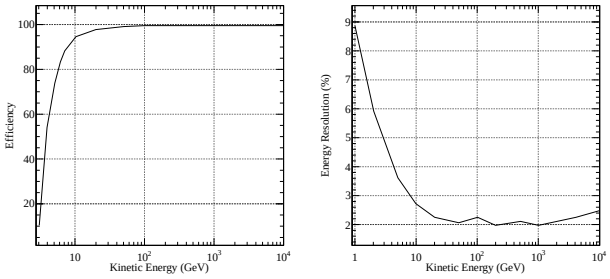

Figure 10: CAL electron detection efficiency (left) and energy resolution (right) [22].

due to CALET's fixed orientation on the ISS with its normal pointing to the zenith limits the statistics at higher energies.

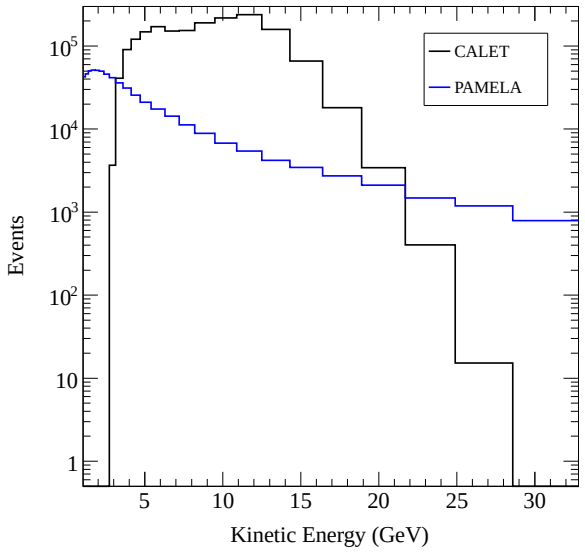

Figure 11: Comparison of expected electron events that would be measured by CALET and PAMELA over a 5 year period.

4 Results

The GCR electron events that CALET and PAMELA would measure over a 5-year period as a function of PAMELA energy bins are shown in Fig. 11, and the positron events that CALET, PAMELA, and AMS-02 would measure over a 5-year period as a function of AMS-02 positron fraction energy bins are shown in Fig. 12. CALET will have superior statistics to PAMELA from ~ 3 GeV to ~ 20 GeV, in the energy range where the positron fraction turns upward, but it will certainly not compete with AMS-02. The CALET measurement will serve as a useful lower energy test of the earth shadow approach that Fermi has utilized for its positron to electron ratio measurements. Comparing CALET's results for this measurement with those from instruments that have magnetic spectrometers will help validate this approach to measure the positron fraction, as well as the technique to measure UH GCR with the CAL utilizing the geomagnetic field [16].

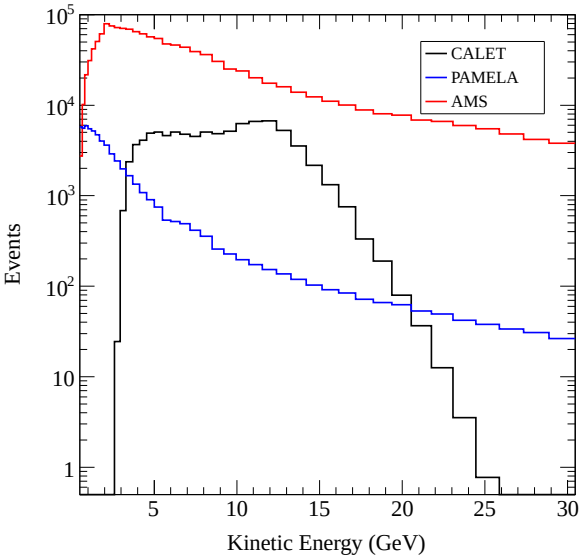

Figure 12: Comparison of expected positron events that would be measured by CALET, PAMELA and AMS-02 over a 5 year period.

Acknowledgment: This work supported at Washington University in St. Louis under NASA Grant NNX11AE02G.

References

[1] J.J. Beatty, et al., Phys. Rev. Lett. 93, 241102, 2004.
[2] M. Aguilar, et al., Phys. Lett. B 646, 145, 2007.
[3] O. Adriani, et al., NAT, 458, 607-609, 2009.
[4] S. Borisov, Astropart. Phys. 34, 1, 2010.
[5] M. Ackermann, et al., PhRvL, 108, 011103, 1-7, 2012.
[6] Aguilar, M., PhRvL, 110, 141102, 1-10, 2013.
[7] Cowsik, R., & Burch, B., PhRvD, 82b, 3009C, 1-7, 2010.
[8] B.F. Rauch for the CALET Collaboration, Predicted CALET Measurements of Electron and Positron Spectra Using the Geomagnetic Field, ASR, 2012 COSPAR Paper E1.15-0053-12, In Review.
[9] S. Torii for the CALET Collaboration, Proc. 33nd ICRC, Paper ID 245, 2013.
[10] M. Mori for the CALET Collaboration, Proc. 33nd ICRC, Paper ID 248, 2013.
[11] A. Moiseev for the CALET Collaboration, Proc. 33nd ICRC, Paper ID 627, 2013.
[12] K. Yoshida for the CALET Collaboration, Proc. 33nd ICRC, Paper ID 735, 2013.
[13] K. Yamaoka for the CALET Collaboration, Proc. 33nd ICRC, Paper ID 1007, 2013.
[14] P.S. Marrocchesi, et al., NIMPA, 659, 477-483, 2011.
[15] P.S. Marrocchesi for the CALET Collaboration, Proc. 33nd ICRC, Paper ID 362, 2013.
[16] B.F. Rauch for the CALET Collaboration, Proc. 32nd ICRC, 6, 348-352, 2011.
[17] B.F. Rauch for the CALET Collaboration, Predicted CALET Measurements of Ultra-Heavy Cosmic Ray Relative Abundances, Advances in Space Research, 2012 COSPAR Paper E1.15-0052-12, In Review.
[18] B.F. Rauch for the CALET Collaboration, Proc. 33nd ICRC, Paper ID 819, 2013.
[19] D.F. Smart & M.A. Shea, AdSpR, 44, 1107-1123, 2009.
[20] O. Adriani, et al., PhRvL, 106, 201101, 1-5, 2011.
[21] V.V. Mikhailov, et al., Bulletin of the Russian Academy of Sciences. Physics, 75, 3, 316-318, 2011.
[22] Y. Akaike, et al., Proc. 32nd ICRC, 6, 364-368, 2011.